Spin-dependent three-dimensional electron momentum density studies in ferromagnetic Co by means of full-scale use of a two-dimensional angular correlation of polarized positron annihilation radiation

1992 J. Phys.: Condens. Matter 4 4595

(http://iopscience.iop.org/0953-8984/4/19/003)

J. Phys.: Condens. Matter 4 (1992) 4595–4611. Printed in the UK

Spin-dependent three-dimensional electron momentum density studies in ferromagnetic Co by means of full-scale use of a two-dimensional angular correlation of polarized positron annihilation radiation

H Kondo†, T Kubota†, H Nakashima†, T Kawano‡ and S Tanigawa†

† Institute of Materials Science, University of Tsukuba, Tsukuba, Ibaraki 305, Japan
‡ Radioisotope Center, University of Tsukuba, Tsukuba, Ibaraki 305, Japan

Received 20 May 1991, in final form 21 January 1992

Abstract. The spin-dependent positron–electron pair momentum density in ferromagnetic cobalt was studied by a full-scale use of the two-dimensional angular correlation of polarized positron annihilation radiation (2D-ACAR) method. Ferromagnetic cobalt shows two different Fermi surfaces, for the majority spins and the minority spins, respectively. The positrons emitted in the positive-beta decay are partially polarized in the direction of their motions. In the present work this property has been utilized. The differences in the 2D-ACAR spectra were observed as a function of spin and their values reached a maximum value of 3%. After the reconstruction the three-dimensional electron momentum density in cobalt in the extended-zone scheme was obtained. The differences in the electron momentum densities represent the contributions of the majority spin and the minority spin, and they showed directional anisotropy. The electron momentum density in the reduced-zone scheme has been obtained by using the LCW-folding procedure. It was found that the electrons in cobalt behaved in the k-space in a two-dimensional manner. The experimental results in the present work were discussed with the theoretical calculations. They showed agreement at the typical symmetry points of the first Brillouin zone except around the point K.

1. Introduction

The positrons emitted in beta decay are spin polarized longitudinally, because the traditional formulation of the conservation of parity is not valid for weak interactions [1, 2]. This property of positive-beta decay was shown by Hanna and Preston in experiments on the angular correlation of positron annihilation radiation [3–5]. The angular correlation of positron annihilation radiation (ACAR) method has been used to obtain the momentum density of the positron–electron pair in solids, and to determine the topology of Fermi surfaces for metallic materials. The polarization annihilation technique has been applied to the study of the electron momentum density distributions and the spin contribution for ferromagnetic materials. Hanna and Preston investigated the ACAR of ferromagnetic materials, iron, nickel, gadolinium and iron–cobalt alloy, as a function of the direction of the applied magnetic fields in 1957 and 1958 [3, 4]. The measurements on an iron single crystal for the [110] and [100] directions were performed by Mijnarends and Hambro in 1964 [6]. They

0953-8984/92/194595+17$04.50

showed that the difference in angular correlations was given by

$$n(\theta) = N_+(\theta) - N_-(\theta) \tag{1}$$

as a function of θ, the deviation between the two emitted photons from 180°, where $N_\pm(\theta)$ are the angular correlations with magnetic fields up or down, respectively. The fact that the measured difference became positive at a small angle was explained in terms of an s–d interaction causing a polarization of the conduction electrons there. The measurements on polycrystalline iron and polycrystalline nickel were performed by Berko and Zuckerman in 1964 [7]. They developed the model for the observed change in the spin of $P(\theta)$ even for an unpolarized conduction band. In the above, $P(\theta)$ is expressed as follows:

$$P(\theta) = (N_\uparrow(\theta) - N_\downarrow(\theta))/(N_\uparrow(\theta) + N_\downarrow(\theta)) \tag{2}$$

where $N_\uparrow(\theta)$ represents an angular correlation with a magnetic field parallel to positron motion, and $N_\downarrow(\theta)$ with a magnetic field antiparallel. The measurements on a single crystal of nickel oriented in the [100], [110] and [111] directions were reported by Mihalisin and Parks in 1966, 1967 and 1968 [8–10]. They suggested that the flat behaviour of $P(\theta)$ in the range $\theta = 0$ to 4 mrad was further evidence against the idea of a conduction band with negative spin polarization. Hohenemser, Weingart and Berko measured the polarized positron annihilation in gadolinium and reported the anisotropic spin alignment of the conduction band [11]. It was stated by the authors that the interpretation of the data in this type of experiment was difficult. Berko and Mills introduced the values of $P_{3\gamma}$ in order to renormalize the 2γ angular correlation experiments and examined the momentum distribution of the spin-aligned electrons in single crystals of gadolinium, iron and nickel [12]. Their results showed anisotropies in these materials and indicated that in the lower momentum range the positrons annihilated with negatively polarized electrons. The experiments mentioned so far were performed by means of the one-dimensional angular correlation of positron annihilation radiation (1D-ACAR) method or the semi-two-dimensional angular correlation of positron annihilation radiation (semi-2D-ACAR) method. These 1D-ACAR or semi-2D-ACAR spectra are the projections of the electron momentum space density integrated over two or one directions, respectively. Recently the three-dimensional electron momentum density has become available by means of the full-scale use of the 2D-ACAR method [13–15]. The three-dimensional momentum space density $\rho(\boldsymbol{p})$ of the positron–electron system can be directly determined from a set of 2D-ACAR spectra followed by the reconstruction technique. This method is a powerful tool in the study of the electron momentum density distribution, the Fermi surface topology and the spin-dependent electron momentum space density. Hoffmann and Berko measured the spin-dependent electron momentum density of gadolinium by this method [13]. In the present work the full-scale use of spin 2D-ACAR results in ferromagnetic cobalt are reported and discussed in a comparison with the theoretical calculations.

2. Experimental details

The experiments were carried out by the 2D-ACAR measurement system, which consists of a pair of detector assemblies of 128 $Bi_4Ge_3O_{12}$ (BGO) scintillators combined

with 128 Hamamatsu R647 photomultiplier tubes individually and a pair of cross-slit systems [14]. The geometrical angular resolution Δ_d is 0.75 mrad × 0.75 mrad at a location of 8 m between each detector assembly and the specimen. One of the detector assemblies automatically moves horizontally and the other automatically moves vertically with a step size of 0.2 mrad, as controlled by programmed stepping motors.

A ^{22}Na source of strength 3×10^9 Bq was used as a positron source and set at a position of 4 mm from the sample. The positrons emitted from ^{22}Na in the positive-beta decay, with energies distributing from 0 to 540 keV, are partially polarized in the direction of the positron motion. The degree of polarization is given by v/c, where v is the velocity of a positron and c is the light velocity. However, the polarization may be smaller than v/c because the polarization also depends on the design of the positron source. We do not refer to the polarization itself here, though it is interesting to study this aspect of the problem. It is certain that the positrons are polarized in our 2D-ACAR system. This polarization of the emitted positrons was utilized in the present work. A magnetic field of 15 kOe was applied along the positron source-sample axis in order to focus the positron beam on the sample and also to polarize the electrons in ferromagnetic cobalt. Cobalt was magnetized up to the saturation level by the magnetic field. A single crystal of cobalt was used as a sample. After the sample was carefully annealed for five hours at 350 °C in a high-vacuum chamber so as not to induce a phase transition, it was placed on a copper holder connected to the cryogenic head with the (0001) plane facing a positron source, and its temperature was held at 26 K during the measurements in order to reduce the effect of the residual momenta of the thermalized positrons.

The smearing effect caused by the thermal behaviour of a positron Δ_t is of the order of 0.22 mrad in FWHM assuming the effective mass of a positron to be twice the mass of a free electron. Another smearing effect, Δ_s, results from the limited size of both the positron beam and the sample. In the present work, Δ_s was determined by the positron beam size of 5.6 mm in diameter, because the sample size was larger than that of the positron beam, and it is of the order of 0.70 mrad. The total resolution from Δ_d, Δ_t and Δ_s is $(\Delta_d^2+\Delta_t^2)^{\frac{1}{2}} = 0.78$ mrad and $(\Delta_d^2+\Delta_t^2+\Delta_s^2)^{\frac{1}{2}} = 1.05$ mrad in the directions parallel and perpendicular to the [0001] axis, respectively. The measurements were performed with a step size of 0.2 mrad × 0.2 mrad in the momentum range ±26 mrad by moving both detectors.

In order to reconstruct the three-dimensional electron momentum density, 2D-ACAR measurements were carried out for seven directions by rotating the sample around the [0001] axis from the $[11\bar{2}0]$ to the $[10\bar{1}0]$ axes with a 5° step. The three-dimensional electron momentum densities have been reconstructed from those measurements followed by the image reconstruction technique based on a direct Fourier transformation.

A pair of measurements for the magnetic fields parallel and antiparallel to the positron motions were carried out for all seven directions, in order to investigate the electron momentum density depending on the electron polarization. Fourteen totally independent 2D-ACAR spectra were measured in the present work. For each 2D-ACAR spectrum 2.3×10^7 counts were accumulated.

3. Data analysis

The 2D-ACAR measurement spectrum

$$N(p_y, p_z) = \int \rho(p)\, \mathrm{d}p_x \tag{3}$$

is the projection of the electron momentum density $\rho(p)$ onto the p_y–p_z plane, where p is the annihilating electron–positron pair momentum. The momentum of the thermalized positron is reduced to almost zero just before the annihilation, so p is thought to almost represent the momentum of the electron. From 2D-ACAR spectra for several different projections we can reconstruct the full three-dimensional momentum density by using the direct Fourier reconstruction technique [14, 15]. This technique is based on the following Fourier projection theorem [16]

$$FT_{-2}[N(p_y, p_z)] \propto B(r)|_{x=0} = (2\pi)^{-3/2} \int\int\int \rho(p) \exp(-\mathrm{i}p \cdot r)\mathrm{d}p|_{x=0} \tag{4}$$

where $B(r)$ is the 3D Fourier transform of $\rho(p)$. The 2D-ACAR data, which were measured along various directions, were Fourier transformed into $B(r)$ by the 2D fast Fourier transform and then the interpolation of $B(r)$ onto a cubic grid was carried out. Finally, the 3D inverse Fourier transform of $B(r)$ yields the full 3D electron momentum density $\rho(p)$. In the reconstruction process the resolution deteriorates by more than 0.1 mrad in all directions. This type of Fourier transformation method has a weak point in the spatial resolution, a so-called 'artefact'. We adopted some special techniques to avoid this phenomenon. Firstly, we took a large angular region, ± 51.2 mrad, in spite of its rather small real distribution within ± 10 mrad. Secondly, an interpolation method based on the third-order polynomials was adopted to enhance the spatial resolution. We examined the Fourier transformation method adopting these techniques. Some of the three-dimensional bodies that were prepared were reconstructed using this method in order to examine the relationship between a reappearance and the numbers of counts and directions in the measurements. We came to be able to reconstruct three-dimensional bodies almost perfectly without the 'artefact' under the condition we found.

In the independent-particle model the full 3D electron momentum density $\rho(p)$ can be described as

$$\rho(p) = \text{const.} \sum_{n,k}^{\text{occ}} \left| \int_V \mathrm{d}r\, \psi_+(r) \psi_{n,k}(r) \exp(-\mathrm{i}p \cdot r) \right|^2 \tag{5}$$

where $\psi_{n,k}(r)$ is the wavefunction of an electron, n is the band index, k is the wave vector, $\psi_+(r)$ is the wavefunction of a thermalized positron ($k = 0$), V is a crystal volume and the summation is taken over all occupied electron states.

To discuss the Fermi surface topology, we reduced the p-space distribution to the k-space one by the Lock–Crisp–West (LCW) [17] folding procedure. The folding procedure is a periodical superposition of $\rho(p)$ on every reciprocal lattice point as given by

$$n(k) = \sum_{G_i} \rho(p + G_i) \tag{6}$$

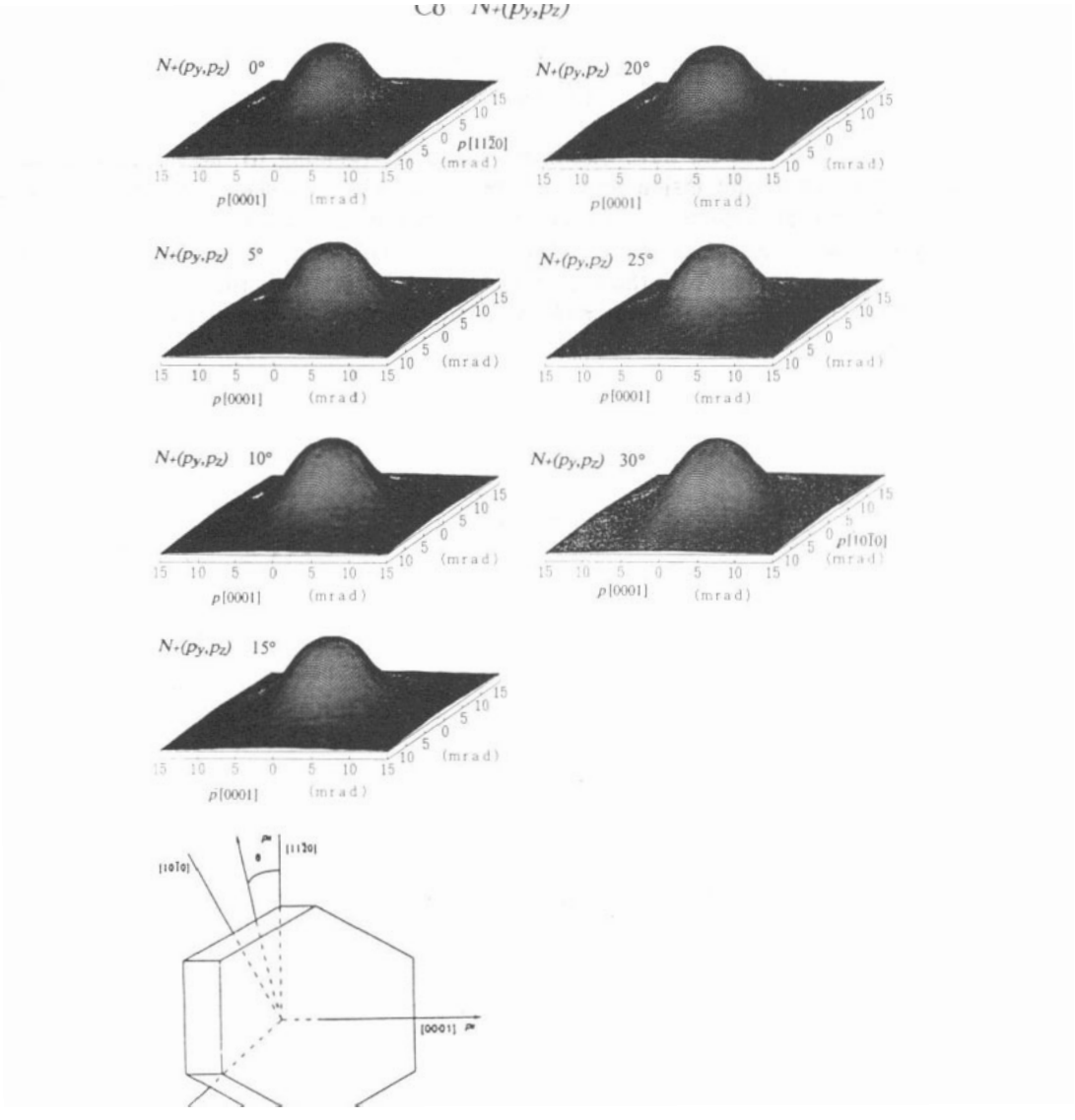

Figure 1. The 2D-ACAR spectra $N_{\pm}(p_y, p_z)$ for seven directions with the magnetic fields parallel to the positron motions. The angles indicated in the spectra correspond to the angles between the integrated axis (p_x) and the a-axis ([11$\bar{2}$0] direction).

where $\boldsymbol{G}_i$ is the ith reciprocal lattice vector and $\boldsymbol{k}$ is the wave vector defined within the first Brillouin zone. Using the Bloch theorem $n(\boldsymbol{k})$ can be described as

$$n(\boldsymbol{k}) = \text{const.} \sum_{n,\boldsymbol{k}} \theta(E_F - E_{n,\boldsymbol{k}}) \int d\boldsymbol{r}_{\text{cell}} \, |\psi_+(\boldsymbol{r})|^2 |\psi_{n,\boldsymbol{k}}(\boldsymbol{r})|^2 \qquad (7)$$

where E_F is the Fermi energy, $E_{n,\boldsymbol{k}}$ is the energy of the electron in the state of

$\psi_{n,k}(r)$ and $\theta(E_F - E_{n,k})$ is a step function expressed as follows:

$$\theta(E_F - E_{n,k}) = \begin{cases} 1, E_F \geqslant E_{n,k} \\ 0, E_F < E_{n,k}. \end{cases} \tag{8}$$

Therefore, $n(k)$ should have discontinuities corresponding to the integral in equation (7) between the inside and outside of the Fermi surface. If the density of positrons can be assumed to be uniform in space, the integral in equation (7) is unity for the occupied electron states. Even in the general case where the density of positrons is not uniform the k-dependence of the integral still seems to be not so large that the discontinuities in $n(k)$ can indicate the location of the Fermi surface in k-space.

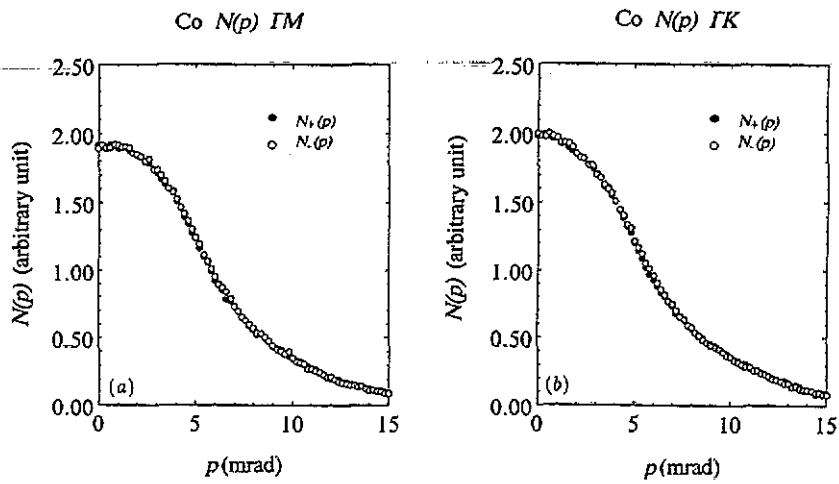

Figure 2. The 2D-ACAR spectra $N_{\pm}(p)$ (*a*) along the ΓM direction and (*b*) the ΓK direction.

4. Results and discussion

The three-dimensional momentum density of the positron–electron pair has been obtained from a set of 2D-ACAR spectra for seven directions using the reconstruction technique. A set of 2D-ACAR spectra $N_+(p_y, p_z)$, which are the counting rates in the magnetic fields parallel to the positron motion, are shown as the bird's eye views in figure 1. These are the projections of the electron momentum density $\rho(p)$ onto the plane in a momentum space perpendicular to the integration axis (p_x). The angle indicated in each figure corresponds to the angle between the $[11\bar{2}0]$ direction (the a-axis) and the integrated direction (p_x). As measured the 2D-ACAR spectra are found to be very featureless, any remarkable anisotropies or structures cannot be seen by the eye unaided. The differences between the spectra parallel to the magnetic field $N_+(p_y, p_z)$ and antiparallel $N_-(p_y, p_z)$ are invisible in the as-measured spectra. The 2D-ACAR spectra $N_{\pm}(p)$ along the two directions, ΓM (the $[11\bar{2}0]$ direction, a-axis) and ΓK (the $[10\bar{1}0]$ direction), are shown in figures 2(*a*) and (*b*), respectively.

The vertical axis indicates the counting rate, and the horizontal axis indicates the momentum as an angle in units of mrad. The full circles represent $N_+(p)$ and the open circles $N_-(p)$. The value of $N(p)$ reaches over 34000 counts around 0 mrad, and 18000 counts around 5 mrad. The statistical errors correspond to 0.54% around 0 mrad, and 0.75% around 5 mrad to the counts. The error bars are not drawn in these figures, since they are rather shorter than the diameter of the circles and not visible. The differences between $N_+(p)$ and $N_-(p)$ are very small, but are found around 0 and 5 mrad in these figures. In order to see the difference in detail, the results of the subtraction of $N_+(p_y, p_z)$ from $N_-(p_y, p_z)$ for the two angles 0 and 30° are shown in figures 3(*a*) and (*b*), respectively. The difference begins to become visible, and it is found that the maximum in the difference spectra is observed around 5 mrad as a bulge and amounts to 3% of the maximum value of the 2D-ACAR spectra. The reason that the difference spectra $N_-(p_y, p_z) - N_+(p_y, p_z)$ were used, rather than $N_+(p_y, p_z) - N_-(p_y, p_z)$, is that it is easy to find a bulge rather than the hollow.

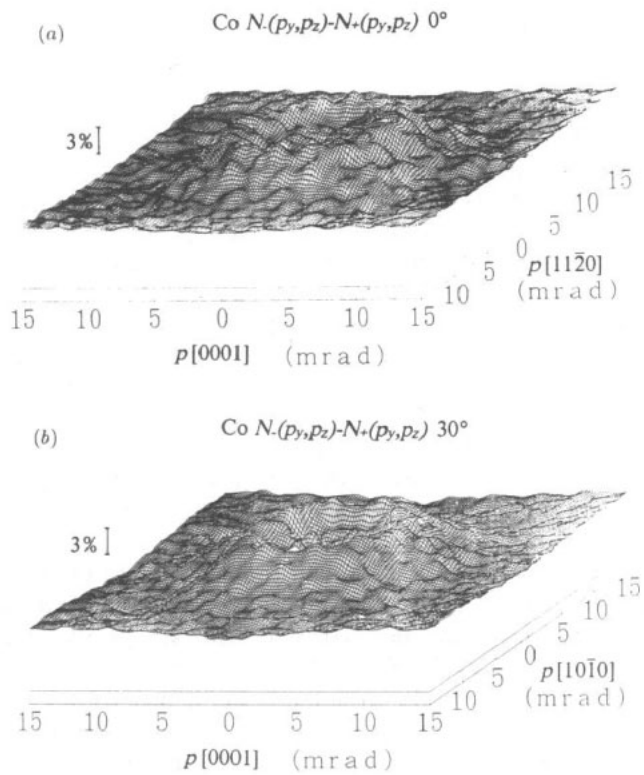

Figure 3. The difference spectra of the subtraction $N_+(p_y, p_z)$ from $N_-(p_y, p_z)$ (*a*) for the angle 0° and (*b*) for the angle 30°.

The difference spectra $N_+(p_y, p_z) - N_-(p_y, p_z)$ along the ΓM and ΓK directions are shown with error bars in figures 4(*a*) and (*b*). As the differences are very small the error bars are long and the data scattered. However, some structure can be found in these profiles. The dips around 5 mrad, which are seen in figures 3(*a*) and (*b*) as bulges, and around 1 mrad, which are rather small, are observed in

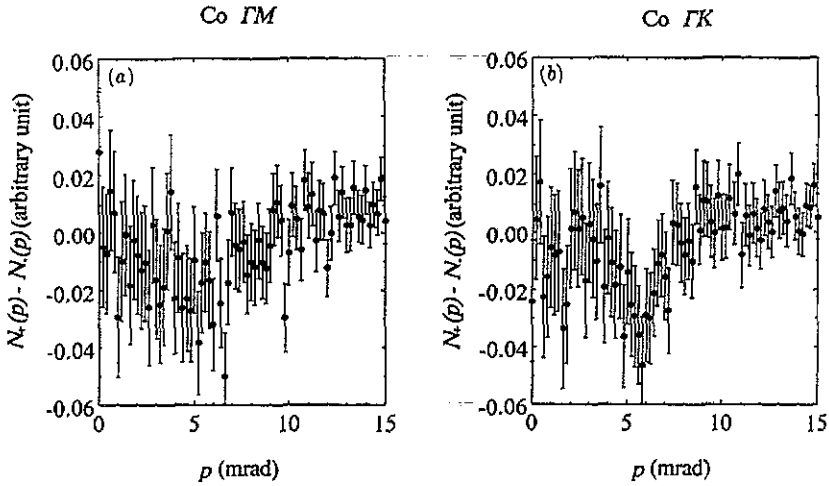

Figure 4. The difference spectra of the subtraction $N_+(p) - N_-(p)$ (*a*) along the ΓM direction and (*b*) along the ΓK direction.

both directions. The normalization of the spectra $N_+(p_y, p_z)$ and $N_-(p_y, p_z)$ is important in the calculation and in the discussion of their sign, positive or negative. We have normalized the spectra using the total number of counts. The same or different normalization methods were adopted in earlier work. It is not sure which normalization method is the best. In the earlier spin-dependent experiments the sign of the difference spectra was the main or the only aspect of the problem discussed. The position where the sign changes will move according to the normalization method. So we shall not refer to the sign but only to the profiles of the difference spectra. In these profiles the main structure is the dip around 5 mrad and this agrees with the fact that the minority-spin Fermi surface is the outer side of the Brillouin zone based on the theoretical calculations.

From the set of measured 2D-ACAR spectra the three-dimensional electron momentum density has been obtained using the reconstruction technique. The results $\rho_+(\boldsymbol{p})$ and $\rho_-(\boldsymbol{p})$ along the three symmetric directions, ΓM, ΓK and ΓA, are shown in figures 5(*a*), (*b*) and (*c*), respectively. The vertical axis indicates the electron momentum space density in arbitrary units, and the horizontal axis indicates the momentum as an angle in units of mrad. The full circles and open circles represent the electron momentum densities where the magnetic fields are parallel and antiparallel to the positron motions, respectively. The full curves in the figures are visual guides.

The angular resolution turns out to be worse by more than 0.1 mrad by the reconstruction process. It is not easy to discuss the statistical error by the reconstruction procedure in detail. However, the statistical error in the reconstruction profiles is thought to be almost the same as that in the original spectra. Because the seven times counts to the original spectra are used in the reconstruction the reappearance with no 'artefact' were already ensured. The statistical error in the reconstructed profiles must be the same as that in the original spectra in the present work. The profiles of the electron momentum densities with both the parallel and antiparallel magnetic fields are roughly the same, and their directional difference is not visible. However the differences between the profiles of the parallel and antiparallel fields can be seen.

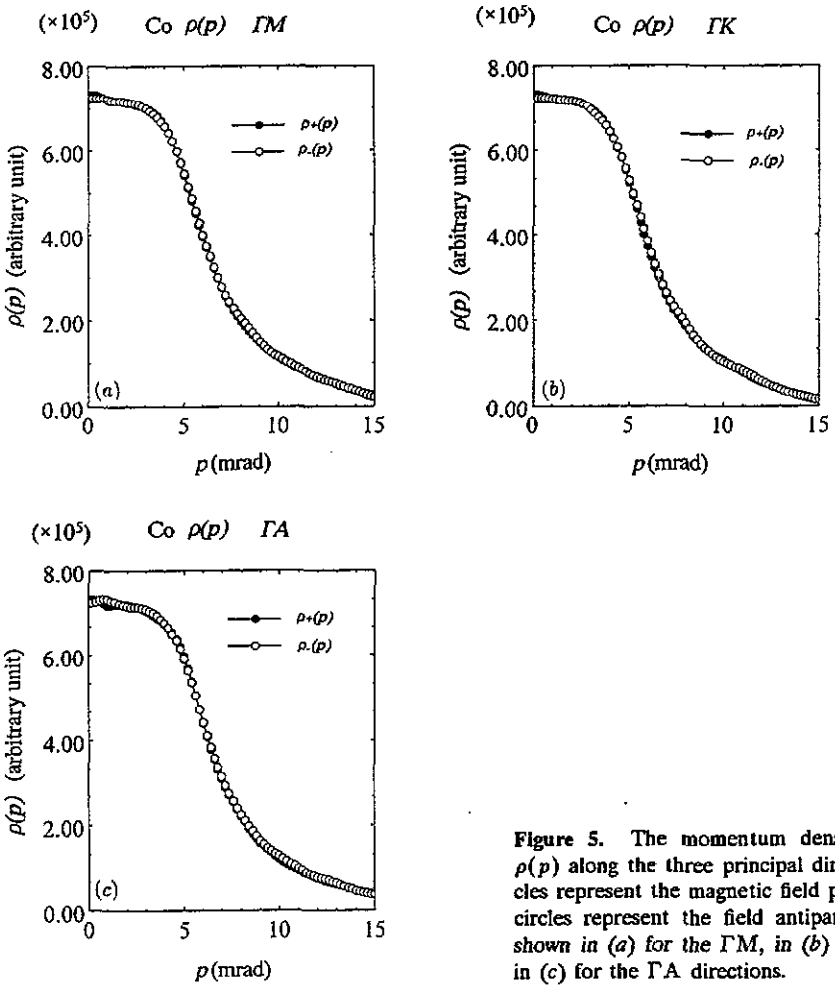

Figure 5. The momentum density distributions $\rho(p)$ along the three principal directions. Full circles represent the magnetic field parallel and open circles represent the field antiparallel. They are shown in (*a*) for the ΓM, in (*b*) for the ΓK and in (*c*) for the ΓA directions.

In order to have a detailed knowledge of these differences, the ratios $P(p)$, which are defined in the following expression and called the polarization, are shown in figures 6(*a*), (*b*) and (*c*) for the principal directions.

$$P(p) = (\rho_+(p) - \rho_-(p))/(\rho_+(p) + \rho_-(p)). \tag{9}$$

The ratio, in the range from 0 to 7 mrad, changes only by a few per cent, and resembles the original spectra. The dips around 1 and 5 mrad in the ΓM and ΓK directions are found, as in the original profiles. In addition, some of the structures are also very similar. Around this momentum range the electron momentum density is high, so the profiles are thought to be significant. These difference profiles will provide the information about the contributions of the majority spins or the minority spins to the electron momentum density distributions. The value of the ratio reaches several per cent in the high-momentum region. This is because of the low electron momentum density and the small denominator in equation (9). Such a fact, obtained by using the ratio in equation (9), was observed in almost all the earlier spin-dependent work.

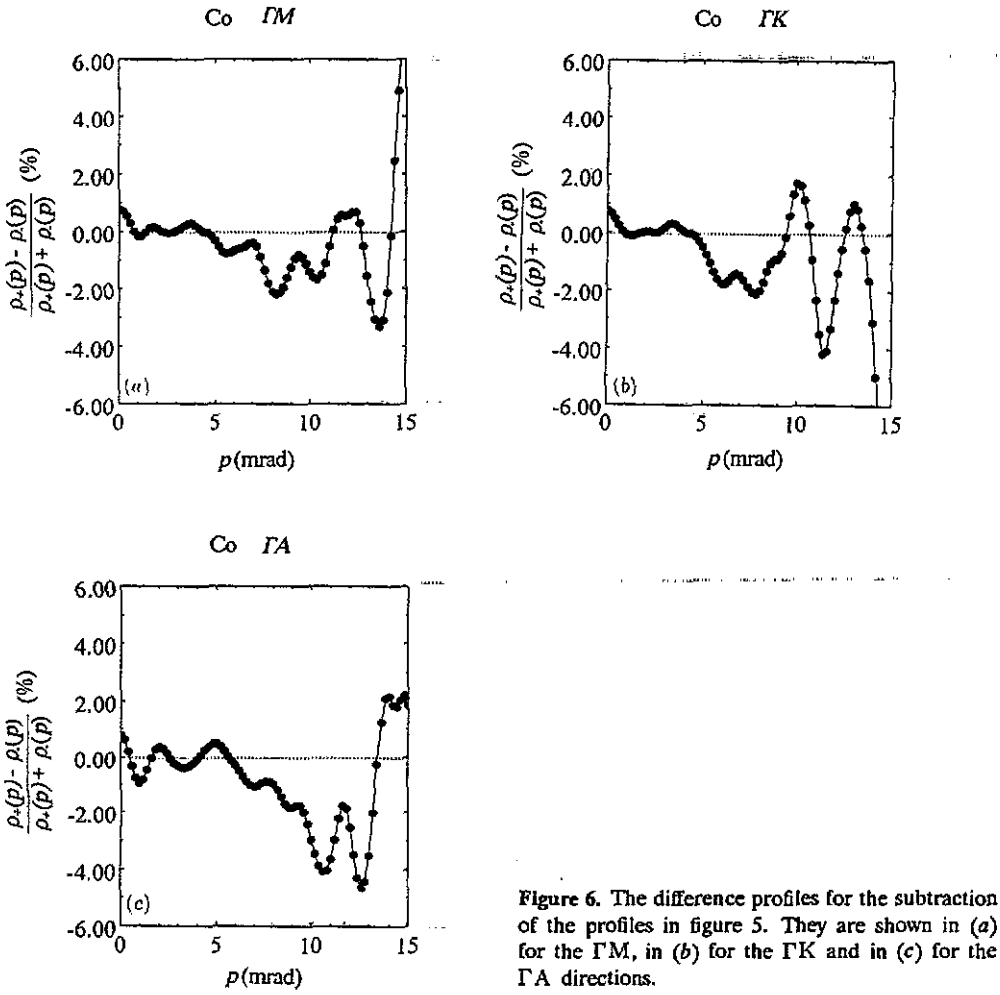

Figure 6. The difference profiles for the subtraction of the profiles in figure 5. They are shown in (*a*) for the ΓM, in (*b*) for the ΓK and in (*c*) for the ΓA directions.

So the ratio in equation (9) is adopted in the present work, although the profiles at this high-momentum region will not be significant.

The electron momentum densities obtained have been expressed in the extended-zone scheme so far. In order to discuss these results in comparison with the theoretical calculations, the electron momentum densities $\rho(p)$ were reduced to the reduced-zone electron momentum densities $n(k)$ by using the LCW-folding procedure. The angular resolution does not change and the statistical error does not come to be worse by using the LCW procedure. The profiles in the high-momentum region in figure 6 become significant in the reduced-zone scheme, because the denominator will not be small there.

The three-dimensional reduced-zone electron momentum densities obtained are shown as the contour maps in figure 7 for the cross sections of the first Brillouin zone (shown in figure 8). The results, where the $n_+(k)$ and $n_-(k)$ with the parallel magnetic field and the one antiparallel to the positron motion, are shown in figures 7(*a*) and (*b*), respectively. The numbers indicated in the maps correspond to the numbers in figure 8, that is (1) , $k_z = \overline{\Gamma A}$; (2), $k_z = \frac{2}{3}\overline{\Gamma A}$; (3), $k_z = \frac{1}{3}\overline{\Gamma A}$; (4),

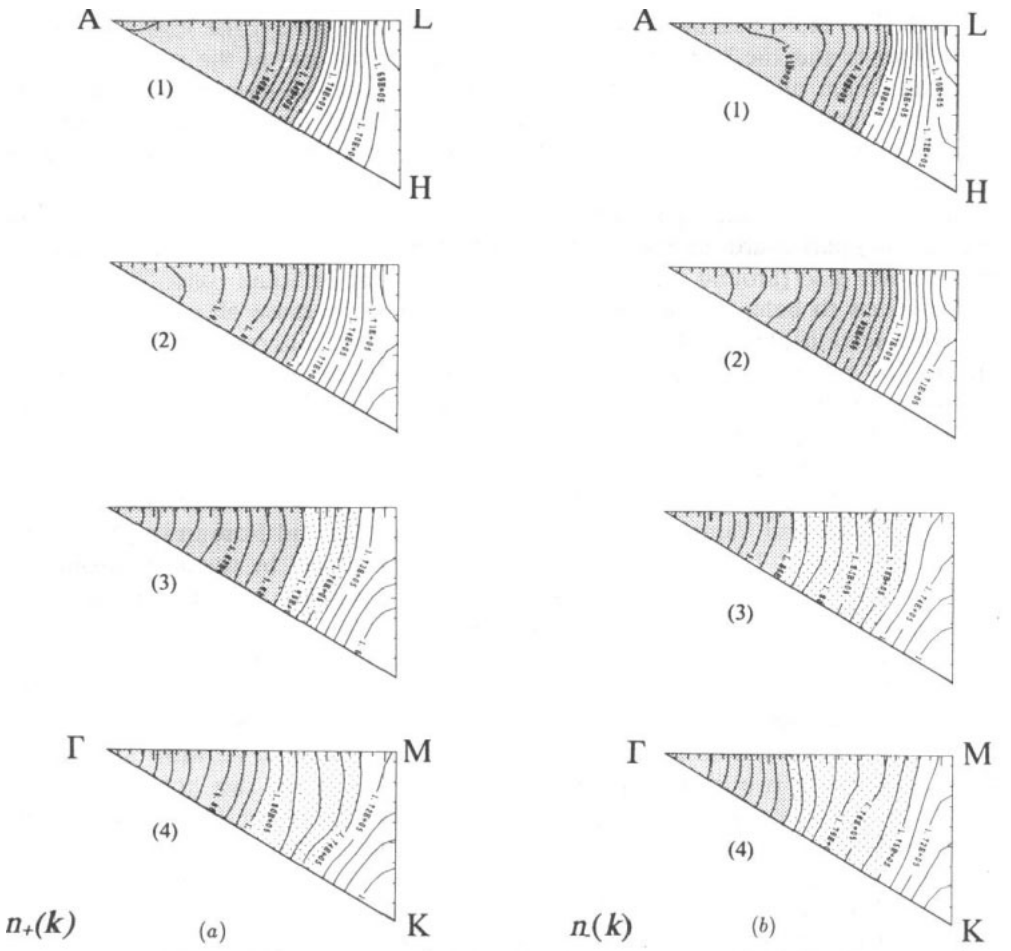

Figure 7. The contour maps of the reduced-zone momentum density for the cross sections of the first Brillouin zone: (*a*) $n_+(k)$ for the parallel magnetic field and (*b*) $n_-(k)$ for the antiparallel one. The numbers indicated beside the contour maps correspond to the numbers shown in figure 8.

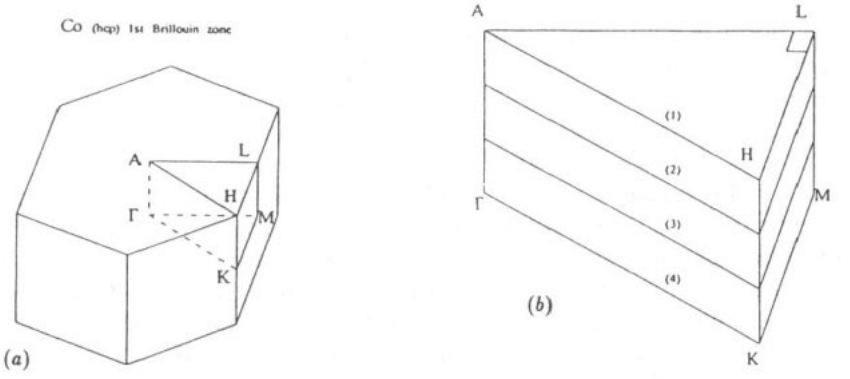

Figure 8. The first Brillouin zone of Co in HCP. The cross sections in the zone, that appear above, are indicated by numbers.

$k_z = 0$. The more heavily shaded parts of the maps represent the high momentum density parts and the boundaries are determined as the loci of the positions of the local maximum of $|\nabla n_{\pm}(k)|$, which is the derivative of the momentum density. In the maps numbered (3) and (4) $|\nabla n_{\pm}(k)|$ has the local maximum at two different loci, so these maps are divided into three parts, two different shaded parts and an unshaded part.

It is found that the appearance of each cross section is roughly similar. The high-density part is around the centre (around the c-axis), and the low-density part is at the outer side (around the KHLM plane), in the first Brillouin zone. The electron in Co seems to behave in a two-dimensional manner, because all contour maps of the cross sections, (1) to (4), are almost the same. Slight differences between $n_+(k)$ and $n_-(k)$ are seen. In order to make the differences clearer, the profiles along the paths, which link the typical symmetry points of the first Brillouin zone, are shown in figures 9(*a*)–(*g*). The full circles represent $n_+(k)$ and the open circles represent $n_-(k)$. The differences are clearly seen.

The band structure and the Fermi surface of cobalt have been calculated by some authors, Wakoh and Yamashita [18], Ishida [19], Batallan and Rosenman [20], Singal and Das [21, 22]. The Fermi surface topologies calculated by them approximately agree with each other. The results in the present work will be compared with the theoretical calculations by Wakoh and Yamashita [18].

In their theoretical calculation there are two electron-like surfaces of the majority-spin band ($e_{11}\uparrow$ and $e_{12}\uparrow$) around the c-axis. The more heavily shaded parts of figure 7 corresponding to high-density parts seem to reflect these surfaces. The theory predicted that there is no minority-spin band around the point A, while around the point Γ there are two large electron-like ($e_9\downarrow$ and $e_{10}\downarrow$) and one hole-like ($h_{10}\downarrow$) surfaces of the minority-spin band. This fact may be one factor for the slight difference in figure 7 between the points A and Γ. The hole-like surfaces of the minority-spin band are around the hexagon ($h_9\downarrow$) and around the point L ($h_5\downarrow$, $h_6\downarrow$ and $h_7\downarrow$). No shaded low-density parts on the outer side of the Brillouin zone seem to reflect these surfaces. The experimental results are consistent with the theoretical calculation so far.

For further detailed discussions the contour maps of the ratios $P'(k)$ given by

$$P'(k) = [n_+(k) - n_-(k)]/[n_+(k) + n_-(k)] \tag{10}$$

are shown in figure 10. The more heavily shaded parts represent the local maximum, and the boundary lines are determined as the positions of the maximum values of differentiation of the ratios $|\nabla P'(k)|$. In the case that $P'(k)$ has the local maximum at more than two places, the maps are divided into three parts, two different shaded parts and an unshaded part. These difference maps are no longer similar to each other. This means that the contributions of the majority spin and of the minority spin to the momentum distirbutions do not show a two-dimensional character. The profiles along the paths linking the typical symmetry points of the first Brillouin zone are also shown in figures 11(*a*)–(*g*). In principle the ratio $P'(k)$ increases at the locations where the electron-like surfaces of the majority-spin band or the hole-like surfaces of the minority-spin band exist. The ratio $P'(k)$ decreases at the locations where the hole-like surfaces of the majority-spin band or the electron-like surfaces of the minority-spin band exist. The dips in the profiles along ΓM and ΓK directions agree with the structure in the original profiles. This is one of the pieces of evidence

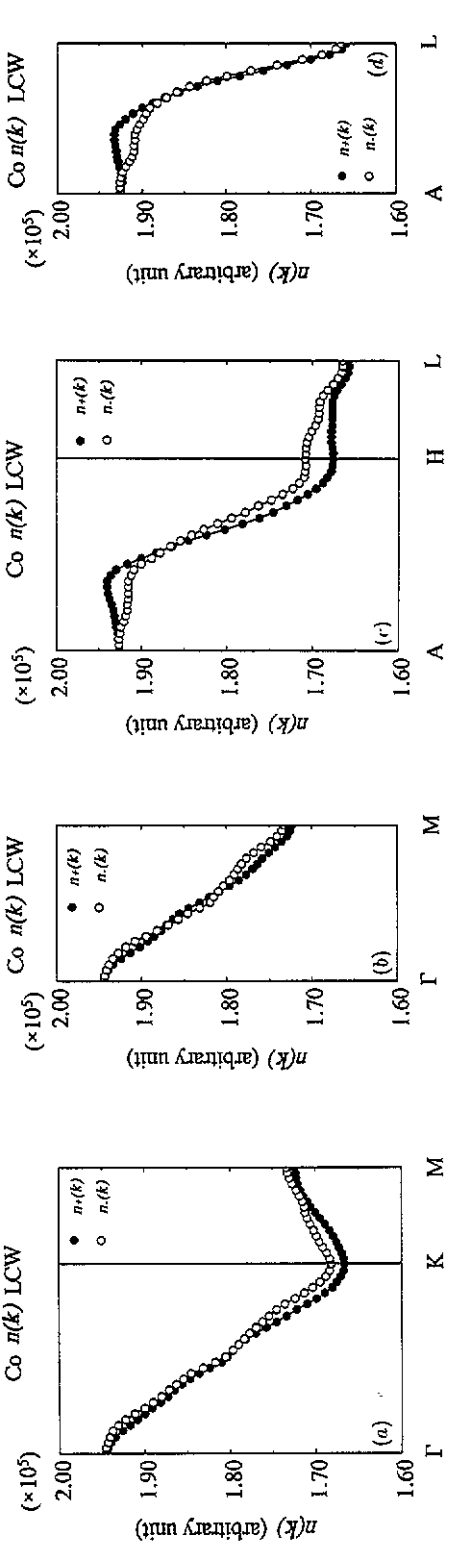

Figure 9. The momentum density profiles along the paths linking the typical symmetry points: (*a*) and (*b*) show the paths in the ΓKM plane; (*c*) and (*d*) show the paths in the AHL plane; (*e*), (*f*) and (*g*) show the paths along the prism edges. Full circles represent $n_+(\boldsymbol{k})$ and open circles represent $n_-(\boldsymbol{k})$.

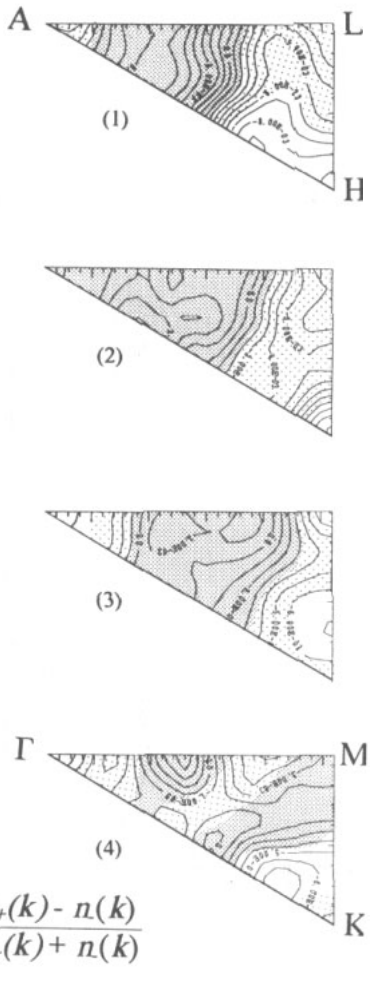

Figure 10. The contour maps for $P'(\boldsymbol{k})$.

that the reappearance is good by the reconstruction and the LCW procedures in the present work. In this discussion only such evident structures are considered.

In the contour map (1) in figure 10 the ratio $P'(\boldsymbol{k})$ is high over a wide area around the point A, although it begins to decrease a little but is still high just at the point A. This agrees with the fact that two electron-like surfaces of the majority-spin band ($e_{10}\uparrow$ and $e_{11}\uparrow$) exist around the point A in the theoretical calculation. The ratio $P'(\boldsymbol{k})$ is high around the point L. This also agrees with the fact that some hole-like surfaces of the minority-spin band ($h_5\downarrow$, $h_6\downarrow$, $h_7\downarrow$ and $h_9\downarrow$) exist around the point L. There are no Fermi surfaces at the point H according to the theoretical calculation, and the ratio $P'(\boldsymbol{k})$ is very low and flat around this point. These facts are consistent. This area becomes small in the contour map (2), but becomes large in the contour maps (3) and (4), not just centred at, but around the edges of the first Brillouin zone.

The value of the ratio $P'(\boldsymbol{k})$ is high at the point Γ. There are two electron-like surfaces of the majority-spin band and two electron-like surfaces of the minority-spin band at the point Γ. There is still one hole-like surface of the minority-spin band in

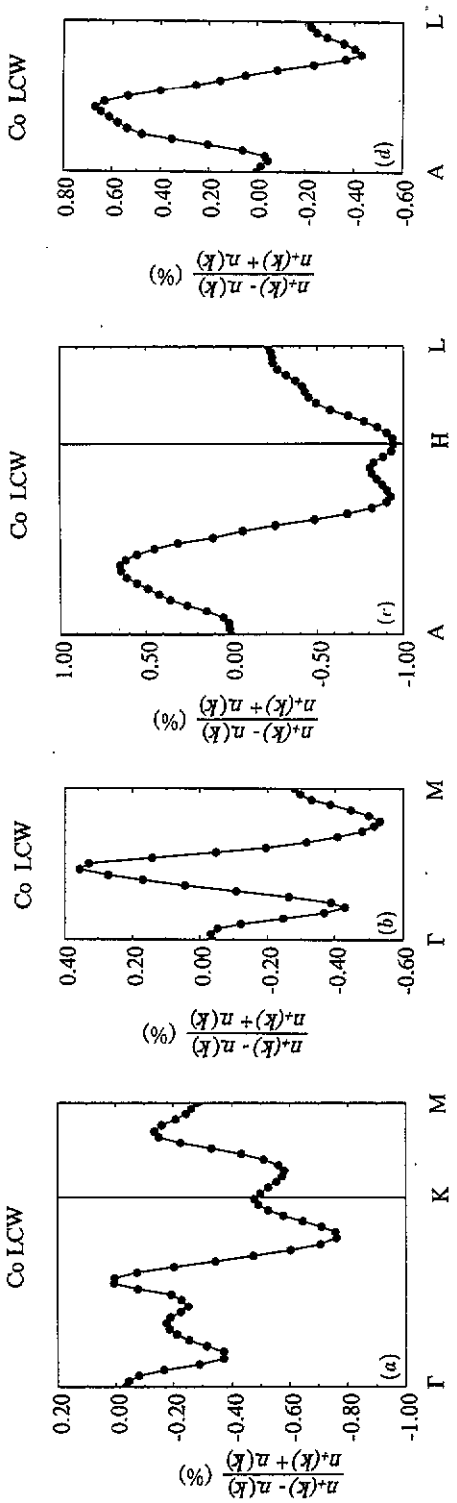

Figure 11. The difference profiles between $n_+(k)$ and $n_-(k)$. (*a*) to (*g*) represent the same paths as in figure 9.

addition to the above electron surfaces. The contribution to the electron momentum densities $n(k)$ from these four electron-like surfaces of the majority- and minority-spin bands seems to be reduced under this approximation, where the contributions to $n(k)$ from each filled band are equivalent. Therefore, the contribution from the hole-like surface of the minority-spin band remains. The high $P'(k)$ part observed around the point Γ seems to reflect this contribution. The size of this hole-like surface is smaller than other electron-like surfaces according to the theory. The low $P'(k)$ part observed just outside of the point Γ seems to reflect the part outside of this hole-like surface. The ratio $P'(k)$ becomes higher again in the more outward parts. The sizes of the two electron-like surfaces of the minority-spin band are smaller than those of the majority-spin band. Only two electron-like surfaces of the majority-spin band exist in the more outward parts. The high $P'(k)$ part seems to reflect this theoretical prediction. There is a hole-like surface of the minority-spin band ($h_9 \downarrow$) around the hexagon. The ratio $P'(k)$ is also high at the points M and K. This fact seems to reflect the contribution of this hole-like surface.

As mentioned above the experimental results agree with the theoretical calculations very well. There is the hole-like connected surface of the minority-spin band around the hexagon, and it is connected except at the point H (the monster $h_9 \downarrow$). However, the low $P'(k)$ parts are observed around the point K, and not just at the point K. This implies that the discontinuities of these surfaces are around the point K. There is only one point in the present work that cannot be explained by the theoretical calculation. The experimental results agree with the theoretical calculations at the point that the hole-like surface of the minority-spin band (the monster $h_9 \downarrow$) are around the hexagon. It is necessary to do theoretical calculations that include a positron wavefunction.

5. Conclusions

The polarized three-dimensional positron–electron pair momentum density of Co has been obtained by means of a full-scale use of 2D-ACAR followed by the reconstruction technique.

The differences between the original spectra $N_+(p)$ and $N_-(p)$ were observed, and the value of the difference spectra amounted to 3% of the maximum. The differences are very small but the structure in the profiles and in the directional anisotropy are found.

The differences between the reconstruction electron momentum densities $\rho_+(p)$ and $\rho_-(p)$ were observed as the polarization parameter $P(p)$ for the three directions in the extended-zone scheme. The structures of the profiles roughly resemble the original subtraction spectra.

Three-dimensional electron momentum densities in the extended-zone scheme were reduced to those in the reduced-zone scheme by using the LCW-folding procedure. It was found that the electron in Co behaves in a two-dimensional manner along the c-axis in the k-space, because the electron momentum density distributions in the cross section perpendicular to the c-axis are nearly the same as each other.

The three-dimensional information related to the contribution of the majority spin and the minority spin were obtained from the ratios $P'(k)$ given in equation (10). The results obtained in the present work were compared with the theoretical calculations. They almost agreed with each other except around the point K in the first Brillouin zone. The theoretical calculation of $\rho_\pm(p)$, $n_\pm(k)$ and $P'(k)$ are very much desired.

Acknowledgments

This work was supported in part by a Grant-in-Aid for Scientific Research from the Japanese Ministry of Education, Science and Culture and by a NEDO Grant for International Co-operative Research.

References

[1] Jackson J D, Treiman S B and Wyld H W Jr 1957 *Phys. Rev.* **106** 517
[2] Page L A and Heinberg M 1957 *Phys. Rev.* **106** 1220
[3] Hanna S S and Preston R S 1957 *Phys. Rev.* **106** 1363
[4] Hanna S S and Preston R S 1958 *Phys. Rev.* **109** 716
[5] Lovas I 1960 *Nucl. Phys.* **17** 279
[6] Mijnarends P E and Hambro L 1964 *Phys. Lett.* **10** 272
[7] Berko S and Zuckerman J 1964 *Phys. Rev. Lett.* **13** 339
[8] Mihalisin T W and Parks R D 1966 *Phys. Lett.* **21** 610
[9] Mihalisin T W and Parks R D 1967 *Phys. Rev. Lett.* **18** 210
[10] Mihalisin T W and Parks R D 1968 *Solid State Commun.* **7** 33
[11] Hohenemser C, Weingart J M and Berko S 1968 *Phys. Lett.* **28A** 41
[12] Berko S and Mills A P 1971 *J. Physique Coll.* **1** 287
[13] Hoffmann K R and Berko S 1982 *Positron Annihilation* ed P G Coleman, S C Shama and L M Diana (Amsterdam: North-Holland) p 325
[14] Suzuki R and Tanigawa S 1989 *Positron Annihilation* ed L Dorikens-Vanpraet, M Dorikens and D Segers (Singapore: World Scientific) p 626
[15] Suzuki R, Osawa M, Tanigawa S, Matsumoto M and Shiotani N 1989 *J. Phys. Soc. Japan* **58** 3251
[16] Berko S 1983 *Positron Solid State Physics* ed W Brandt and A Dupasquier (Amsterdam: North-Holland) p 64
[17] Lock D G, Crisp V H and West R N 1973 *J. Phys. F: Met. Phys.* **3** 561
[18] Wakoh S and Yamashita J 1970 *J. Phys. Soc. Japan* **28** 1151
[19] Ishida S 1972 *J. Phys. Soc. Japan* **33** 369
[20] Batallan F and Rosenman I 1975 *Phys. Rev.* B **11** 545
[21] Singal C M and Das T P 1977 *Phys. Rev.* B **16** 5068
[22] Singal C M and Das T P 1977 *Phys. Rev.* B **16** 5093